ADVANCED THEORY AND SIMULATIONS
www.advtheorysimul.com

Determining the Potential of Maximum Entropy from Ab Initio Molecular Dynamics

*Amanda S. Petersen, Thor K. Madsen, Theophilus K. Sarpey, Christian M. Schott, Elena L. Gubanova, Adrian V. Himmelreich, Aliaksandr S. Bandarenka, and Jan Rossmeisl**

Understanding electrochemical interfaces at the atomic level is essential for optimizing catalytic performance in energy conversion and storage technologies. This study introduces a computational framework based on ab initio molecular dynamics (AIMD) simulations to predict the potential of maximum entropy (PME) a descriptor of electric double layer disorder and charge transfer efficiency. By integrating AIMD with the generalized computational hydrogen electrode, it is systematically investigated how electrolyte composition, cation identity, and pH effect the position of PME. The approach reproduces experimental shifts in PME for Au and Pt electrodes and provides unprecedented insights into the emergence of multiple PME values in mixed-cation systems. The findings challenge conventional models of electrolyte structuring by revealing the presence of multiple PME values within mixed-cation systems. This suggests a more complex interplay between cations, adsorbates, and interfacial disorder than previously assumed. The computational framework developed in this study provides a predictive tool for understanding these interactions, offering new strategies for tuning electrocatalytic activity.

1. Introduction

Electrochemical energy conversion and storage are critical technologies for future energy solutions.[1–3] The energy conversion itself takes place at the interface between the electrolytes and electrodes through intricate electrochemical reactions in the electric double layer (EDL). A fundamental understanding of the atomic-scale interactions in these interfaces is imperative to achieve high-performing electrocatalysts.[4–10] Consequently, exploring the influence of altered electrolyte compositions and electrode surfaces on the electrocatalytic reactions becomes crucial.

While electrolyte composition and pH are well-known macroscopic parameters affecting electrocatalytic activity, their influence on the microscopic ordering of interfacial water and adsorbates remains an area of research.[11–24] Despite the relatively weak interactions between metal surfaces and water molecules, summarized research findings have shown that the interfacial water layers considerably control the electrochemical processes.[11–14] When the interfacial water structure is well-organized, more energy is required to rearrange the water dipoles after a mass or charge transfer. In contrast, at the potential of maximum entropy (PME), the interfacial water molecules exhibit maximal orientational disorder, such that the reactant species and electrons can pass through the EDL relatively readily, as the water molecules can reorient more easily.[25] As a result, the closer the PME is to a reaction's thermodynamic equilibrium potential, the faster the reaction should be. Consequently, the PME can be regarded as the predominant reason for energy barriers that hinder mass and charge transfers through the interface. In **Figure 1**, this concept is illustrated, inspired by.[26]

A. S. Petersen, T. K. Madsen, J. Rossmeisl
Department of Chemistry
Center for High Entropy Alloy Catalysis
University of Copenhagen
Universitetsparken 5, Copenhagen Ø 2100, Denmark
E-mail: jan.rossmeisl@chem.ku.dk

The ORCID identification number(s) for the author(s) of this article can be found under https://doi.org/10.1002/adts.202500958

DOI: 10.1002/adts.202500958

T. K. Sarpey, C. M. Schott, E. L. Gubanova, A. V. Himmelreich, A. S. Bandarenka
Physics Department
Physics of Energy Conversion and Storage
Technical University of Munich
James-Franck-Straße 1, Garching, 85748 Bei München, Germany

T. K. Sarpey
Materials Research Department GSI Helmholtz Centre for Heavy Ion Research GmbH
Planckstraße 1, 64291 Darmstadt, Germany

A. S. Bandarenka
TUM Catalysis Research Center
Technical University of Munich
Ernst-Otto-Fischer-Straße 1, Garching, 85748 Bei München, Germany

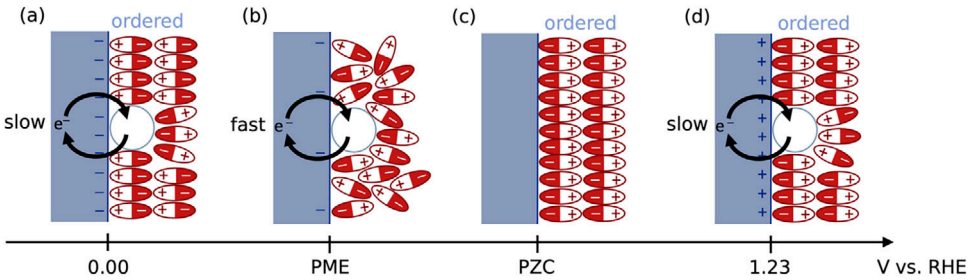

Figure 1. Scheme of the orientation of the interfacial water molecules as the dipoles at the electrode surface depend on the applied potential. a) The interfacial water molecules tend to orient with the hydrogens toward the electrode surface when the electrode is negatively charged. b) At the PME, the interfacial water layer has the highest disorder in the EDL. c) At the PZC, there is no excess charge on the electrode surface. However, the oxygen atoms of the water molecules tend to point toward the electrode surface due to the specific interaction between the oxygen atom and the (uncharged) metal surface. d) When the electrode is positively charged, the interfacial water molecules tend to orient with the oxygen toward the electrode surface. Grey circles represent adsorbed species (e.g., intermediates) at the electrode surface.

As shown in Figure 1, the electrode surface charge varies with the applied potential, and the potential of zero charge (PZC) represents the specific potential where no excess charge exists on the electrode surface (Figure 1c). The PME is often closely related to the PZC but occurs at a slightly more negative potential.[25] This shift arises from strong directional interactions between the oxygen atoms of the interfacial water molecules and the d-orbitals of the transition metal surface.[27] A more negative potential is required to offset this specific interaction and achieve maximal disorder in the EDL.

While PME has been extensively measured using laser-induced current transient (LICT) techniques,[28–31] a predictive theoretical framework based on first-principle calculations has remained elusive. In this work, we introduce a computational approach that combine ab initio molecular dynamics (AIMD) simulations with the generalized computational hydrogen electrode (GCHE) framework[32–35] to predict PME values. By systematically examining the effects of electrolyte composition, cation identity, and pH, we demonstrate that our method accurately reproduces experimentally observed PME shifts for Au and Pt electrodes.[12,26,36]

Two studies by X. Ding et al.[26,36] as well as a study by T. K. Sarpey et al.[12] on PME measurements serve as the experimental validation of our computational model. In the first study, Ding et al. examined how alkali metal (AM) cations influence the PME positions on a polycrystalline platinum (Pt_{pc}) electrode, correlating PME shifts with cation hydration energies and catalytic activities.[36] They further investigated the pH dependence on the PME position of polycrystalline gold (Au_{pc}) electrodes in contact with either 0.5 M Na_2SO_4 or K_2SO_4, revealing two significantly different pH dependencies. Sarpey et al.[12] extended this analysis by measuring PME of Au_{pc} in contact with mixed Na_2SO_4/K_2SO_4 electrolytes, demonstrating catalytic tunability of the oxygen reduction reaction (ORR).

While modeling PZC remains an active area of research,[37–42] a thorough PME study using ab initio grand canonical approaches has, to our knowledge, yet to be reported.[43] Our study aims to fill this gap in research and advance the understanding of the electrochemical interface in the context of the PME. Our study seeks to shed light on the intricate interplay between atomic-scale structure and electrocatalytic properties, providing valuable insights for the continuous development of high-performing electrochemical devices.

2. Results and Discussion

To systematically predict the PME, we developed a computational framework based on ab initio molecular dynamics (AIMD) simulations, combined with the GCHE approach. This method allows us to determine the stability of different interface compositions and predict the PME as an emergent property of the electrochemical system. Our approach is schematically shown in **Figure 2**.

AIMD simulations are performed using density functional theory (DFT) to capture the dynamic behavior of the electrochemical interface at a finite temperature. The interfacial system is modeled with explicit water molecules and AM cations to replicate experimental conditions. An ensemble of interface structures is generated from which the work functions and associated energetics are sampled. For each interface composition, a normal distribution is fitted with the work function as an order parameter, as a result, yielding a hypothetical PME. To establish if the PME of each work function distribution is probable, the most stable interface composition at a given potential is calculated from the sampled energetics. If the work function distribution of the composition falls within this potential region, the peak of the work function distribution, $\bar{\phi}_{e^-}$, is considered a possible PME.

In the model, the PME is constant on the standard hydrogen electrode (SHE) potential scale because the work function is linked directly to the reversible hydrogen electrode (RHE) and SHE by

$$eU_{RHE} = \phi_{e^-} - \phi_{SHE} + 2.303k_B T \cdot pH \quad (1)$$

where ϕ_{SHE} is the work function of the electrode at pH = 0 and $U_{SHE} = 0$ V.[44,45] Since the equation imposes constrains on the macroscopic interface, it is expected to hold in the limit of large unit cells. While unit cell size effects were not explicitly evaluated in this study, we assume that the chosen unit cell is sufficiently large to capture the essential electrochemical interface behavior, making the unit cell representable for the interface as a whole. Here, a 3×4 unit cell with three atomic layers is used, with 24 mobile water molecules above the surface. To maintain constant water density throughout the simulation, an additional hexagonal

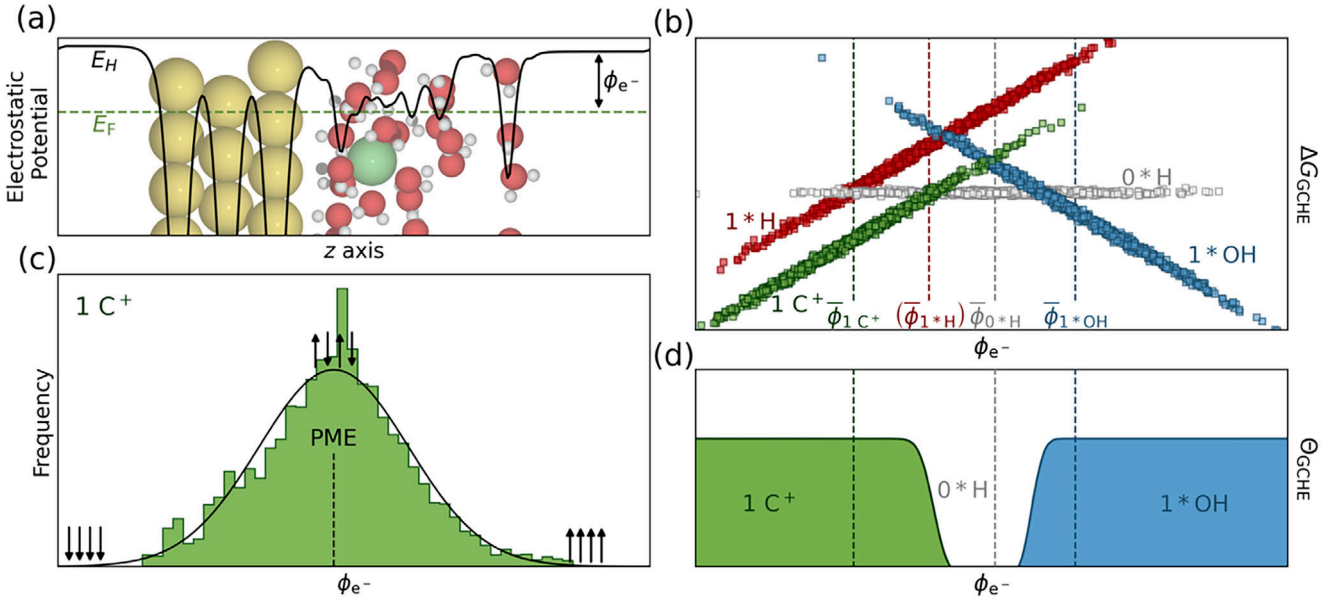

Figure 2. An overview of the methodology for obtaining the possible PMEs. a) Snapshot of an AIMD simulation plotted with the Hartree potential (black, solid line) and the Fermi level (green, dashed line). The work function is the difference between the vacuum level on the right side and the Fermi level. The boundary conditions are periodic in the plane and nonperiodic, with a dipole correction[51] out of the plane. b) GCHE phase plot of a model system. Each line corresponds to the interface composition labeled. Each data point is a snapshot in the MD simulation. The work function means, $\bar{\varphi}$, are additionally marked for each composition with the dashed lines. If the mean of the work function distribution is in an energetically favorable potential window, it is regarded as a possible PME; otherwise, it is denoted with parentheses. c) Histogram of calculated work functions obtained directly from the AIMD sampling. A normal distribution is fitted from which the PME is obtained as the distribution peak. The water dipole orientations are exemplified with the black arrows. C^+ designates the cation in question (e.g., 1 C^+ is one cation in question). d) The absolute derivative of the Boltzmann-weighted mean from the Pourbaix plot in (b) as a function of potential, resulting in an interface composition plot. The work function distribution peaks that are possible PMEs are marked with dashed lines.

layer of six water molecules is placed on top. The computational details are further described in Section S1 (Supporting Information).

From the AIMD simulations, the work function can be obtained from the planar-averaged electrostatic potential and the Fermi level, E_F, using

$$\phi_{e^-} = \left\langle E_H\left(z_{max}\right)\right\rangle - E_F \tag{2}$$

$$E_H(z) = \int_{x,y} E_H(x, y, z)\, dx\, dy \tag{3}$$

where $E_H(x, y, z)$ is the electrostatic potential, which is calculated for each structure by DFT. The planar-averaged electrostatic potential of an image of an AIMD simulation is shown in Figure 2a. In addition, the *xy*-plane electrostatic potential profiles at three representative *z*-coordinates – the Pt surface, the fixed interfacial water layer, and the vacuum, region where the work function is sampled – are provided in Figure S1 (Supporting Information), demonstrating the negligible variation across the plane.

The net dipole moment of the water layer is the result of the integrated dipole moment in the direction normal to the surface, which is influenced by the orientation of water molecules, by electronic countercharges, and by the positions of ions. If all configurations of the electrolyte molecules can be produced in a representative manner, the AIMD simulation, without any external charge, should result in a normal distribution with the work function as the order parameter, from which we obtain the PME as the mean. In this study, we found that such a normal distribution is obtained with 1200 steps. Accordingly, all PME analyses presented here and in the SI are based on the last 1200 snapshots of each AIMD trajectory. Such a work function distribution is shown in Figure 2c. As seen in the Supporting Information (Figure S2, Supporting Information), the work function distribution converges within a relatively brief period, indicating reorientation occurs often and with negligible energy barriers.

As schematically shown in Figure 2c by the arrows, there are only a few microstates for which all water dipoles point in a specific direction. In contrast, there are many microstates in which the dipoles of the water molecules approximately cancel perpendicular to the surface. Consequently, the peak of the distribution indicates which macrostate of the net dipole moment has the highest multiplicity and, therefore, provides a statistical definition of the PME.

The PME is thus closely related to the most probable work function value, since this corresponds to the configuration with the largest number of interfacial water dipole arrangements. This statistical interpretation captures the entropic origin of the PME. However, whether the most probable work function indeed constitutes the PME of a given interface composition must also be consistent with the system's thermodynamics. To account for this, we evaluate the energetics of the sampled states within the GCHE framework, which ensures that the PME corresponds not only to the entropic maximum but also to an interface composition that is thermodynamically accessible at the given pH.[32,34]

Within the GCHE, explicit simulations of the interface can be evaluated in a phase diagram at a specified pH value, since the

potential and chemical potential of the interface species are expressed by work function and the associated energetics.

$$\Delta E_{GCHE}\ (n,\ x,\ \phi_{e^-}, pH) = E\left(n,\ x,\ \phi_{e^-}\right) - \langle E(\ \{n,\ x\} = 0)\rangle - x\left(\mu_{C^+(aq)} + k_B T \cdot \log\left(\left[C^+\right]\right)\right) - n\frac{1}{2}\mu^{\circ}_{H_2} - n\left(\phi_{SHE} - \phi_{e^-} - 2.303 k_B T \cdot pH\right) \quad (4)$$

The energy, ΔE_{GCHE}, is a function of the number of protons n added to or subtracted from the cell, the number of cations x in the interface region, the work function, the cation concentration $[C^+]$, and pH. In this study, $x = \{0, 1, 2\}$ and $n = \{-6 \cdots 6\}$ with the unit cell consisting of 12 surface atoms, but these values could vary depending on the investigated system. μ denotes the chemical potential of the cation in question, $C^+(aq)$, and H_2 (g) at standard conditions, obtained from calculations and thermodynamic tables.[46] k_B is the Boltzmann constant, T is the absolute temperature, and $\langle E(\ \{n, x\ \} = 0)\rangle$ is the reference energy. The energetics of the cations are referenced to the most stable oxide of the cation in question,[47] as an attempt to mimic the positive charge of the cation in the interface.[48] Setting the energetics of the AM cations is discussed in Section S2 (Supporting Information).

This approach allows us to evaluate the most stable structures in a Pourbaix interface diagram at a given potential,[49] as exemplified in Figure 2b. For any given potential, electrolyte composition, pH, and electrode, the structural properties can be weighted as Boltzmann-weighted means, allowing us to determine the probable interfacial structures. In Figure 2d, the most stable interface compositions are plotted as the absolute derivative of the Boltzmann-weighted means as a function of work function. If the peak of the work function distribution falls within the potential window in which the interface compositions is the most stable, the mean is regarded as a possible PME.

In general, DFT calculations of quantities such as energy barriers and binding energies are subject to inherent errors.[50] A binding energy error would lead to a vertical shift of each composition line in Figure 2b. However, because our approach relies on DFT energies only to assess the relative stability of interface compositions – and not their absolute values – the impact of such errors is mitigated. Moreover, the PME is determined by the mean work function of 1600 MD iterations, making it less sensitive to numeric inaccuracies. If we were to include more water molecules in the simulations, the resulting work function distribution would become sharper, while preserving the mean value. While this method is inherently more robust than direct DFT-calculated quantities, its accuracy still depends on DFT correctly identifying the most stable interfacial composition at a given potential.

One approach to determine PME experimentally is to use the LICT technique.[29–33,40–42] In this method, a short-time laser pulse induces a small heating of the interface under potential control. This thermal probing shifts the interface toward a higher entropy microstate. The following relation explains the shift;

$$\frac{\partial U}{\partial T_q} = \frac{\partial \Delta S}{\partial q_T} \quad (5)$$

where q is the surface charge on the electrode, and U is the electrode potential. This is derived for an ideal polarizable electrode from the electrocapillary equation.[29,52] (Equation 4) is used to identify the potential of zero potential transient, which translates into the PME. Using a potentiostat and a three-electrode setup, U can be assumed to be constant, and (Equation 4) translates into a current transient, where the current relaxation is monitored as the system returns to its starting temperature and initial EDL state. Current transient peaks with a negative sign are observed if the electrode surface is negatively charged at that specific potential. In contrast, the current transient peaks are positive if the surface is positively charged. As a result, at the PME, the relaxation peaks are minimal, as the initial and final states are close to one another in terms of the interface order.

2.1. Catalytic Activity: Influenced by the Potential of Maximum Entropy

In their study on Pt_{pc}, X. Ding et al. demonstrated how the presence of the AM cation in the electrolyte impacts the activities of ORR and the hydrogen evolution reaction (HER).[26] The activity results from the study are summarized in **Figure 3**a,b, where the HER and ORR activities are displayed versus the measured PME values for Pt_{pc}. It was observed that by changing the AM cations in the electrolyte from Li^+ toward Cs^+, the PME values were specifically shifted further away from the thermodynamic equilibrium potential of the HER (0.00 V vs RHE), as seen in Figure 3a. Consequently, this shift results in a decrease in the HER activity. Conversely, when changing the AM cations from Li^+ toward Cs^+, the PME values approach the thermodynamic equilibrium potential of the ORR (1.23 V vs RHE), which leads to an increase in the ORR activity. This trend is illustrated in Figure 3b. These findings highlight a strong correlation between the HER and ORR activities on Pt_{pc} and the degree of order in the EDL. Besides, Huang et al. studied the cation-dependent HER/hydrogen oxidation reaction (HOR) activity as well and came to a similar conclusion, attributing the change to the structure-making and, respectively, structure-breaking properties of those ions, referring to the Marcus-Hush-Chidsey formalism.[53] Nevertheless, the effect of the AM cations on the electrocatalytic reactions on Pt_{pc} may be explained qualitatively and quantitatively by the PME.

This further demonstrates how the properties of the AM cations have a significant impact on the structure of the EDL. It is plausible to assume that the loss of interfacial order for higher hydration energies at potentials close to the HER's onset potential results in an increase in HER activity. Lower hydration energies, on the other hand, result in a loss in interfacial order at a potential far from the HER potential, which in turn increases the activity toward the ORR. These results strongly suggest that the EDL structure at the interface is affected by interactions between cations and water molecules and results in a different degree of order at the same potential. As a result, the nature of the cations can control the PME's location and, consequently, influence the electrocatalytic activities.

In Figure 3c,d, a linear relationship between the PME values and the hydration energy of the AM cations is shown. Measurements of PMEs of Au_{pc} are also included in Figure 3d. These

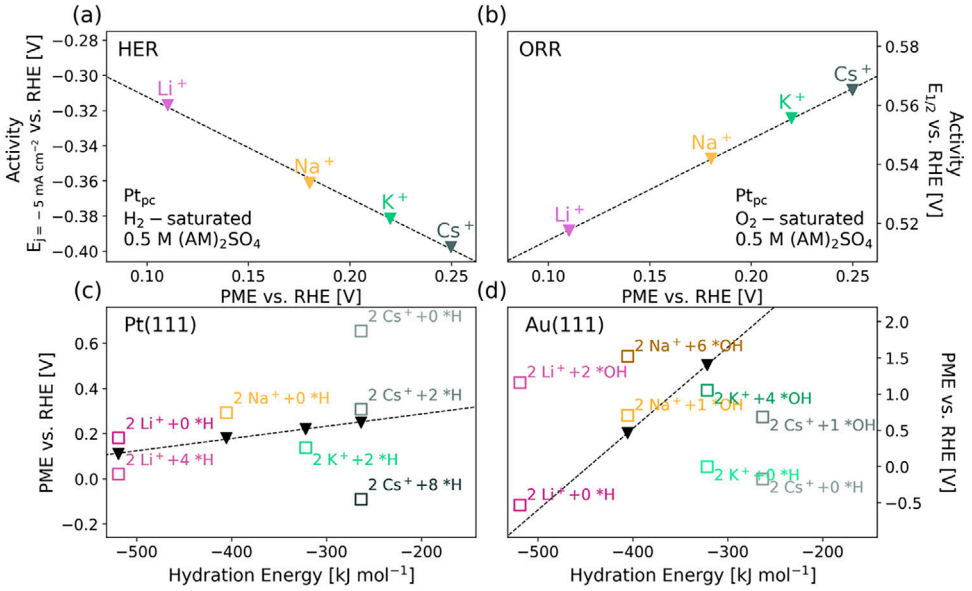

Figure 3. Overview of experimental findings from ref. [26] displayed with computationally modeled PMEs at pH = 6. a) The potential required for a current density of −5 mA cm^{-2} of Pt_{pc} against the PME value of the studied AM cation. b) The half-wave potentials of Pt_{pc} versus the PME values in the case of the associated AM cations. These results imply that the HER activity gets enhanced by AM cations with higher hydration energies, whereas, for the ORR, we find the reverse trend. These experimentally measured PME values are co-plotted with computationally modeled PME values (open symbols) for (c) Pt(111) and (d) Au(111). In (c), the PME values exhibit a linear trend with the hydration energies in reasonable agreement with modeled PMEs. For Au(111), a similar agreement is shown in (d).

are extracted from an additional study by X. Ding et al.[36] Also provided are computed work function peak positions for both Pt(111) (Figure 3c) and Au(111) (Figure 3d). This demonstrates how the EDL is significantly influenced by the AM cations' identity and how the cation in question affects the structure of the EDL. Interestingly, as shown for Pt in Figure 3c, a linear relationship is revealed when plotting the PME values against the hydration energy of the AM cations. In Figure 3d, a straight line is drawn between the PME values of Au to suggest a probable trend.

To enable the comparison with experimentally measured PME values for Au_{pc} and Pt_{pc} in Figure 3, AIMD simulations were performed for Au(111) and Pt(111) facets in contact with an interfacial region containing up to two AM cations, of which the work function distribution have been plotted in SI for Au(111) (Figures S3 and S4, Supporting Information) and for Pt(111) (Figures S5 and S6, Supporting Information). Simulations containing three cations were found to be unstable and are thus not considered. The labels in Figure 3c,d indicates the cations and associated work function peaks. For pH 6, the most stable interface compositions were obtained by grouping the work function in bins of size 4 meV, and subsequently, Boltzmann-weighed the GCHE energy for the different interface compositions in each bin. In general, the experimentally determined PMEs fall within the proximity of at least one work function distribution. For both Pt(111) and Au(111) surfaces, the calculated work function distributions suggest two AM cations in the interface with only a minor quantity of $^*H$ or $^*OH$ adsorbed near the PMEs. In contrast to Au, where the PME is in a region with adsorbed $^*OH$, the estimated work function distributions indicate that $^*H$ should be adsorbed on Pt in the vicinity of the PME.

The offset in the modeled work function peak positions may be due to the consideration of only even-numbered $^*H$ adsorption on Au(111). The impact of $^*H$ coverage on work function peak position is explored in the SI for the different AM cations on Pt(111) (Figure S4, Supporting Information) and Au(111) (Figure S5, Supporting Information). In general, only a slight change is observed. In addition, different compositions of the modeled interface could have the same charge but different configurations, e.g., pure water is equal in charge to adsorbed $^*H$ and $^*OH$ but could energetically be more stable and possibly change the work function peak position. How different coverages of $^*OH$ significantly alter the work function peak position is summarized in Figures S6 and S7 (Supporting Information) for Pt(111) and Au(111), respectively.

2.2. pH and Cation Effects on the Potential of Maximum Entropy of Au(111)

To further validate the computational method for predicting PME values, the study of Au_{pc} electrodes in 0.5 M Na_2SO_4 and 0.5 M K_2SO_4 by X. Ding et al.[36] was modeled at various pH values. The experimentally measured PMEs are shown as black markers in **Figure** 4b for Na^+ and in Figure 4d for K^+ at comparable pH values.

For Au_{pc} in the 0.5 M Na_2SO_4 solutions (Figure 4b), the PME values gradually move toward more positive potentials with increasing pH. However, for the Au_{pc} electrode in 0.5 M K_2SO_4 electrolytes (Figure 4d), a rapid change in PME position is observed when changing the pH from 4 to 6. This indicates that a slight change in pH within this pH region can have a significant

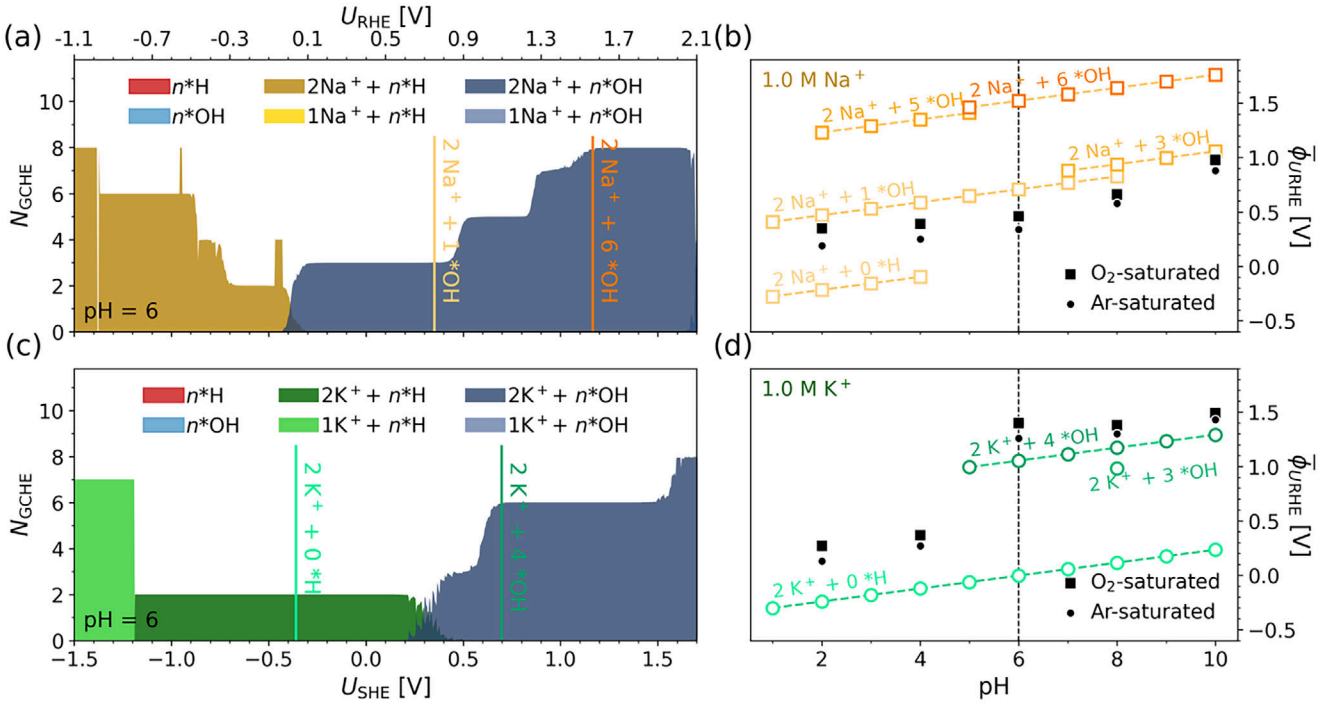

Figure 4. Calculated and experimentally measured PMEs as a function of pH. a) and c) show interface compositions of Au(111) in contact with an electrolyte containing 1.0 M Na^+ (a) or 1.0 M K^+ (c) at pH 6. In general, AM cations are present in the interface in this potential range. As the potential is shifted toward more positive values, *OH starts to adsorb. The possible PMEs are marked as vertical lines for the composition as labeled. In (b) and (d), the possible PMEs are co-plotted with experimental PMEs (black markers) as a function of pH. The square and circle black markers signify experimental data obtained using electrolytes saturated with different gases.

impact on the EDL structure. X. Ding et al. hypothesized that specific adsorption, such as *OH and sulfate adsorption, could result in phase transitions and interfacial water rearrangements in the EDL,[54] which consequently would shift the PME location. They also noted an effect depending on whether the carrier gas is Ar- or O_2-saturated, which was not included in the current simulations for simplicity.

The interface composition plots in Figure 4a,c, show the composition of interfaces containing 1.0 M Na^+ (Figure 4a) and K^+ (Figure 4c), respectively, at pH 6. These composition plots, which are derived from Pourbaix diagrams, demonstrate how the coverage of *OH increases with more positive potentials in both Na^+- and K^+-containing electrolytes. To systematically explain the abrupt changes in the PME location and EDL structure observed experimentally, the stable work function distributions were sampled as a function of pH in Figure 4b,d. Within the GCHE, changing the pH shifts the energetics of the associated interface compositions, and the work function distributions move accordingly on the RHE scale. As a result, peaks of the work function distribution, $\bar{\phi}_{e^-}$, that were previously unlikely may now become stable and probable in certain potential regions.

The computationally modeled work function distributions are co-plotted with the experimental PMEs in Figure 4b for Na^+ and Figure 4d for K^+. At specific pH values, multiple work function distributions are found to be stable in both electrolytes. However, these findings are not supported by the experimental results. For the Na^+-containing system in acidic conditions (Figure 4a,b), the model suggests the work function distribution corresponding to 2 Na^+ cations with 1 *OH adsorbate can account for the experimentally observed PMEs. As the pH increases, a continuous shift is predicted, with 3 *OH becoming the most stable adsorbate coverage in this potential range.

In the K^+-containing electrolyte (Figure 4c,d), a second probable work function distribution emerges around pH 5 as the pH changes from acidic to neutral conditions. This distribution corresponds to an interface composition with 2 K^+ cations and 4 *OH adsorbates. The specific adsorption of sulfate with varying degrees of protonation was also considered in the AIMD simulations, but they were not found to be stable. In contrast, the adsorption of *OH appears to explain the abrupt shift in experimentally measured PMEs and supports that K_2SO_4 and Na_2SO_4 cannot be treated as equivalent supporting electrolytes, as their EDL properties at the same pH are significantly different, which can impact the electrocatalytic activity, as shown in Figure 3a,b.

2.3. Observations of Multiple Potentials of Maximum Entropy

Our analysis of the PME reveals the possibility that an interface system can exhibit multiple PME values. In a recent study, Sarpey et al. investigated the effects of mixing 0.5 M Na_2SO_4 and 0.5 M K_2SO_4 electrolytes in contact with an Au_{pc} electrode at pH 8, reporting a quasi-linear shift in PME.[12] In **Figure 5**a, we reproduce their original analysis for comparison.

However, a closer examination of the underlying LICT measurements suggests that this quasi-linear trend may oversimplify

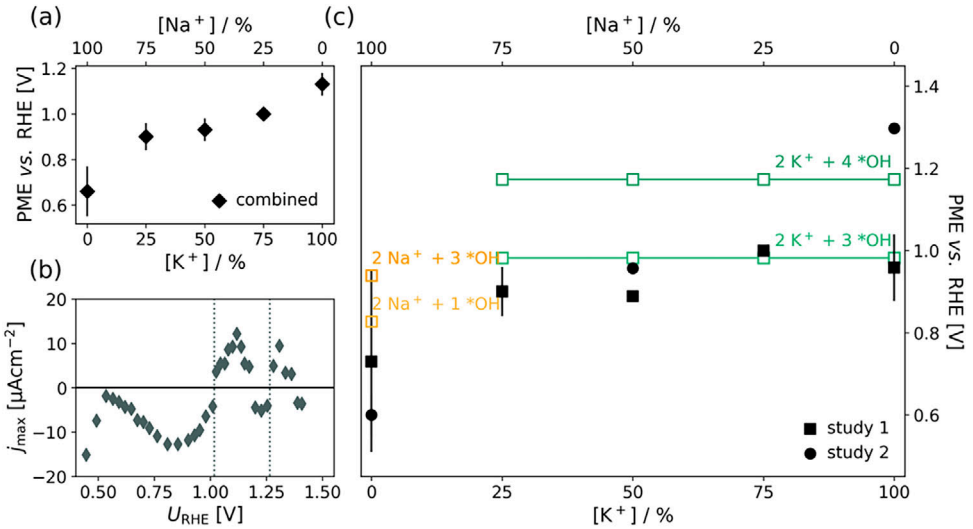

Figure 5. Calculated and measured PME values for mixtures of 1.0 M Na^+ and 1.0 M K^+ in various ratios. a) Depicts the combined PMEs as a function of AM cation concentration, adapted with permission from ref. [12] In (b), the PMEs of (a) are separated into individual PME values (black markers) and co-plotted with calculated PMEs as a function of cation concentrations. The LICT sweep of 1.0 M K^+ is represented in (c), with permission from ref. [12] PME per sweep is given by the negative to positive zero-crossing of the sweep, highlighted with the dashed lines. Since the pH of 8 is constant, the PME positions are not subjected to change.

the complexity of the system. If we analyze the two individual LICT data sets separately, instead of averaging the PME positions, we observe that for 1 M K^+, two distinct PME values emerge. This observation is further supported by the LICT sweep data presented in Figure 5b, which clearly shows two potentials where the current density, *j*, transitions from negative to positive.

To gain deeper insights, we have represented the calculated work function distributions as a function of Na^+ and K^+ concentrations in Figure 5c, alongside the experimental unaveraged LICT measurements. In the GCHE framework, the AM cation concentration is modified by adjusting the concentration in (Equation 5). Our analysis suggests that Na^+ cations are typically stable in the interface only when K^+ is absent from the electrolyte. As the K^+ concentration increases, the Na^+ states become unstable, leading to the emergence of PME values associated with the presence of two K^+ cations in the interface.

We have also included AIMD simulations of systems with 1:1 ratios of Na^+ and K^+ cations in our analysis. However, the interface energies for these mixed-cation systems were found to be less favorable than those involving two identical cations. Due to limitations in our simulation setup, particularly the system size and number of atoms, our analysis is constrained to the 1:1 cation ratio. It is, however, plausible that other cation ratios could be more energetically favorable, potentially stabilizing mixed-cation states in the interface.

Comparing the computational PME values to the experimental measurements in Figure 5c, we find that they generally agree. As the K^+ concentration increases, the Na^+ cations disappear from the interface, resulting in PME values corresponding to configurations involving 2 K^+ + 3 *OH, as well as an additional PME associated with 2 K^+ + 4 *OH. However, as the K^+ concentration approaches 25% 1 M, a slight discrepancy emerges between the calculated and experimental work function distributions. While simulations of multiple cation ratios and states between 2 *OH and 3*OH adsorbates would in principle provide a more complete picture, such calculations are computationally prohibitive with the present AIMD setup, as they would require larger cell sizes and extensive sampling to ensure adequate statistics. Instead, we focus on the 1:1 Na^+/K^+ mixture, which represent the most competitive case for cation in the interface. Intermediate ratios are expected to yield PME values interpolating between the Na^+- and K^+-dominated limits, such that the essential physics is already captured by the 1:1 mixture. Indeed, comparison with experiment (Figure 5c) supports this interpretation, although small deviations may arise from the finite-size limitations of the simulations or form additional phenomena such as interfacial cation segregation; rather than forming a homogeneous mixture, the cations may preferentially cluster into spatially distinct Na^+- or K^+-rich interfacial domains. Such segregation would lead to an apparent linear combination of PME values when measured experimentally. On the other hand, the large error bars of the experimental values at the ratio 1:0 as well as the large discrepancy of the two distinct experimental datasets at 0:1 might also indicate the overall rather high instability of the real-world system raising the possibility of measurement errors. Furthermore, as the K^+ concentration reaches 1 M, a second PME value appears in the LICT measurements near the configuration of 2 K^+ + 4 *OH. Again, a discrepancy is noted, likely due to the inability of our systems to capture states between 4 *OH and 5 *OH adsorbates.

In summary, the identification of multiple PMEs within a single electrolyte composition suggests that multiple stable configurations may exist for distinct ion concentrations, challenging the traditional assumption of a single global PME per system. Moreover, considering the work of Sarpey et. al.[12] and present results, it can be assumed that several PMEs may exist, but only one of them coincides with the PZC, as the PME is a function of specific adsorption for certain systems. This finding underscores the need for a more nuanced understanding of the com-

plex interplay between ions, adsorbates, and work function at the metal/electrolyte interface.

3. Conclusion

This study introduces a robust computational framework integrating AIMD simulations in the GCHE framework to predict the PME at electrochemical interfaces. By bridging atomic-scale modeling with experimental validation, we provide a predictive tool for understanding the fundamental relationship between interfacial structure, electrolyte composition, and electrocatalytic properties.

A key finding of this work is the identification of multiple PME values in mixed-cation systems, an insight that was further supported by the reanalysis of experimental data. This discovery challenges the traditional assumption of a single global PME per system, revealing that under certain electrolyte compositions, multiple stable configurations can exist, each corresponding to a distinct PME value, whereof one of the PMEs coincides with the PZC.

Moreover, our findings underscore the significant impact of alkali metal cations on PME positions and the resulting electrocatalytic activity, particularly for the HER and ORR. By accurately quantifying interface compositions at measured PMEs, our method offers a powerful tool for unraveling complex electrochemical environments and guiding the rational design of catalyst-electrolyte interfaces.

The computational approach developed in this study not only aligns with experimental findings but also extends the capability to explore and predict the behavior of electrochemical interfaces at the atomic scale. This advancement paves the way for more precise control and optimization of electrochemical processes, contributing to the development of next-generation materials and devices for sustainable energy applications.

Supporting Information

Supporting Information is available from the Wiley Online Library or from the author.

Acknowledgements

The authors would like to thank the Center for High Entropy Alloy Catalysis (CHEAC), funded by the Danish National Research Foundation (DNRF 149), financial support from the European Union under ERC Synergy grant DEMI, Grant Agreement No. 101118768, and the Villum Foundation through the Center for the Science of Sustainable Fuels and Chemicals (#9455). A.S.B. and J.R. also thank Deutsche Forschungsgemeinschaft (DFG) for the funding via Collaborative Research Center (CRC), SFB 1625. A.S.B. acknowledges DFG in the framework of the project BA 5795/8-1.

Conflict of Interest

The authors declare no conflict of interest.

Data Availability Statement

The data that support the findings of this study are openly available in [calc_PME] at https://erda.ku.dk/archives/9ea424752d66ba2276957718fc240315/published-archive.html, reference number [1].

Keywords

Ab initio molecular dynamics, electric double layer, electrocatalysis, generalized computational hydrogen electrode, oxygen Reduction Reaction

Received: May 26, 2025
Revised: August 29, 2025
Published online:

[1] R. Schlögl, *Top. Catal.* **2016**, *59*, 772.
[2] B. Dunn, H. Kamath, J.-M. Tarascon, *Science* **2011**, *334*, 928.
[3] P. De Luna, C. Hahn, D. Higgins, S. A. Jaffer, T. F. Jaramillo, E. H. Sargent, *Science* **2019**, *364*, aav3506.
[4] P. Sebastián-Pascual, A. S. Petersen, A. Bagger, J. Rossmeisl, M. Escudero-Escribano, *ACS Catal.* **2021**, *11*, 1128.
[5] A. Bagger, I. E. Castelli, M. H. Hansen, J. Rossmeisl, in *Handbook of Materials Modeling*, (Eds.: W. Andreoni, S. Yip), Springer International Publishing, Cham **2020**, pp. 1473.
[6] A. Bagger, L. Arnarson, M. H. Hansen, E. Spohr, J. Rossmeisl, *J. Am. Chem. Soc.* **2019**, *141*, 1506.
[7] C. M. Schott, P. M. Schneider, K.-T. Song, H. Yu, R. Götz, F. Haimerl, E. Gubanova, J. Zhou, T. O. Schmidt, Q. Zhang, V. Alexandrov, A. S. Bandarenka, *Chem. Rev.* **2024**, *124*, 12391.
[8] A. S. Bandarenka, M. T. M. Koper, *J. Catal.* **2013**, *308*, 11.
[9] S.-J. Shin, D. H. Kim, G. Bae, S. Ringe, H. Choi, H.-K. Lim, C. H. Choi, H. Kim, *Nat. Commun.* **2022**, *13*, 174.
[10] J.-M. McGregor, J. T. Bender, A. S. Petersen, L. Cañada, J. Rossmeisl, J. F. Brennecke, J. Resasco, *Nat. Catal.* **2025**, *8*, 79.
[11] X. Ding, T. K. Sarpey, S. Hou, B. Garlyyev, W. Li, R. A. Fischer, A. S. Bandarenka, *ChemElectroChem* **2022**, *9*, 202101175.
[12] T. K. Sarpey, A. V. Himmelreich, K.-T. Song, E. L. Gubanova, A. S. Bandarenka, *Small Sci.* **2024**, *4*, 2400042.
[13] T. Kobina Sarpey, E. Keles, E. L. Gubanova, A. S. Bandarenka, *Bandarenka in Encyclopedia of Solid-Liquid Interfaces*, Elsevier, Amsterdam **2024**, pp. 43–58.
[14] C.-Y. Li, J.-B. Le, Y.-H. Wang, S. Chen, Z.-L. Yang, J.-F. Li, J. Cheng, Z.-Q. Tian, *Nat. Mater.* **2019**, *18*, 697.
[15] A. H. Shah, Z. Zhang, Z. Huang, S. Wang, G. Zhong, C. Wan, A. N. Alexandrova, Y. Huang, X. Duan, *Nat. Catal.* **2022**, *5*, 923.
[16] G. A. Kamat, J. A. Zamora Zeledón, G. T. K. K. Gunasooriya, S. M. Dull, J. T. Perryman, J. K. Nørskov, M. B. Stevens, T. F. Jaramillo, *Commun. Chem.* **2022**, *5*, 20.
[17] A. S. Varela, W. Ju, T. Reier, P. Strasser, *ACS Catal.* **2016**, *6*, 2136.
[18] J. Zheng, W. Sheng, Z. Zhuang, B. Xu, Y. Yan, *Sci. Adv.* **2016**, *2*, 1501602.
[19] W. Sheng, H. A. Gasteiger, Y. Shao-Horn, *J. Electrochem. Soc.* **2010**, *157*, B1529.
[20] X. Chen, I. T. McCrum, K. A. Schwarz, M. J. Janik, M. T. M. Koper, *Angew. Chem. Int. Ed.* **2017**, *56*, 15025.
[21] J. Hussain, H. Jónsson, E. Skúlason, *ACS Catal.* **2018**, *8*, 5240.
[22] Z. W. Seh, J. Kibsgaard, C. F. Dickens, I. Chorkendorff, J. K. Nørskov, T. F. Jaramillo, *Science* **2017**, *355*, aad4998.
[23] M. Luo, M. T. M. Koper, *Nat. Catal.* **2022**, *5*, 615.
[24] E. Zhen, Y. Chen, J. Huang, *J. Chem. Phys.* **2025**, *162*, 144702.
[25] A. Ganassin, P. Sebastián, V. Climent, W. Schuhmann, A. S. Bandarenka, J. Feliu, *Sci. Rep.* **2017**, *7*, 1246.
[26] X. Ding, D. Scieszka, S. Watzele, S. Xue, B. Garlyyev, R. W. Haid, A. S. Bandarenka, *ChemElectroChem* **2022**, *9*, 202101088.
[27] S. Trasatti, *J. Electroanal. Chem. Interfacial Electrochem.* **1974**, *150*, 1.
[28] V. Climent, B. A. Coles, R. G. Compton, *J. Phys. Chem. B* **2001**, *105*, 10669.

[29] V. A. Benderskii, G. I. Velichko, *J. Electroanal. Chem. Interfacial Electrochem.* **1982**, *140*, 1, https://doi.org/10.1016/0368-1874(82)85295-7.
[30] D. Scieszka, J. Yun, A. S. Bandarenka, *Mater. Interfaces* **2017**, *9*, 20213.
[31] A. Auer, F. J. Sarabia, D. Winkler, C. Griesser, V. Climent, J. M. Feliu, J. Kunze-Liebhäuser, *ACS Catal.* **2021**, *11*, 10324.
[32] M. H. Hansen, J. Rossmeisl, *J. Phys. Chem. C* **2016**, *120*, 29135.
[33] M. H. Hansen, A. Nilsson, J. Rossmeisl, *Phys. Chem. Chem. Phys.* **2017**, *19*, 23505.
[34] J. Rossmeisl, K. D. Jensen, A. S. Petersen, L. Arnarson, A. Bagger, M. Escudero-Escribano, *J. Phys. Chem. C* **2020**, *124*, 20055.
[35] J. Rossmeisl, K. Chan, R. Ahmed, V. Tripković, M. E. Björketun, *Phys. Chem. Chem. Phys.* **2013**, *15*, 10321.
[36] X. Ding, B. Garlyyev, S. A. Watzele, T. Kobina Sarpey, A. S. Bandarenka, *Chem. A Eur. J.* **2021**, *27*, 10016.
[37] S. Sakong, A. Groß, *J. Chem. Phys.* **2018**, *149*, 084705.
[38] L. S. Pedroza, A. Poissier, M.-V. Fernández-Serra, *J. Chem. Phys.* **2015**, *142*, 034706.
[39] S. Duan, X. Xu, Z.-Q. Tian, Y. Luo, *Phys. Rev. B* **2012**, *86*, 045450.
[40] S. Schnur, A. Groß, *Physics* **2009**, *11*, 125003.
[41] S. R. Kelly, H. H. Heenen, N. Govindarajan, K. Chan, J. K. Nørskov, *J. Phys. Chem. C* **2022**, *126*, 5521.
[42] J. Le, M. Iannuzzi, A. Cuesta, J. Cheng, *Phys. Rev. Lett.* **2017**, *119*, 016801.
[43] A. Shandilya, K. Schwarz, R. Sundararaman, *J. Chem. Phys.* **2022**, *156*, 014705.
[44] S. Trasatti, *J. Electroanal. Chem. Interfacial Electrochem.* **1986**, *209*, 417.
[45] D. M. Kolb, *Angew. Chem., Int. Ed.* **2001**, *40*, 1162.
[46] J. K. Nørskov, J. Rossmeisl, A. Logadottir, L. Lindqvist, J. R. Kitchin, T. Bligaard, H. Jónsson, *J. Phys. Chem. B* **2004**, *108*, 17886.
[47] A. Jain, S. P. Ong, G. Hautier, W. Chen, W. D. Richards, S. Dacek, S. Cholia, D. Gunter, D. Skinner, G. Ceder, K. A. Persson, *APL Mater.* **2013**, *1*, 011002.
[48] J. T. Bender, A. S. Petersen, F. C. Østergaard, M. A. Wood, S. M. J. Heffernan, D. J. Milliron, J. Rossmeisl, J. Resasco, *ACS Energy Lett.* **2023**, *8*, 657.
[49] H. A. Hansen, J. Rossmeisl, J. K. Nørskov, *Phys. Chem. Chem. Phys.* **2008**, *10*, 3722.
[50] B. Kanungo, A. D. Kaplan, C. Shahi, V. Gavini, J. P. Perdew, *Phys. Chem. Lett.* **2024**, *15*, 323.
[51] L. Bengtsson, *Phys. Rev. B* **1999**, *59*, 12301.
[52] J. A. Harrison, J. E. B. Randles, D. J. Schiffrin, *J. Electroanal. Chem. Interfacial Electrochem.* **1973**, *48*, 359.
[53] B. Huang, R. R. Rao, S. You, K. Hpone Myint, Y. Song, Y. Wang, W. Ding, L. Giordano, Y. Zhang, T. Wang, S. Muy, Y. Katayama, J. C. Grossman, A. P. Willard, K. Xu, Y. Jiang, Y. Shao-Horn, *JACS Au* **2021**, *1*, 1674.
[54] J. Tymoczko, V. Colic, A. S. Bandarenka, W. Schuhmann, *Surf. Sci.* **2015**, *631*, 81.